NANO LETTERS

pubs.acs.org/NanoLett Letter

Observation of the Time-Reversal Symmetric Hall Effect in Graphene−WSe_2 Heterostructures at Room Temperature

Priya Tiwari, Divya Sahani, Atasi Chakraborty, Kamal Das, Kenji Watanabe, Takashi Taniguchi, Amit Agarwal,* and Aveek Bid*

Cite This: https://doi.org/10.1021/acs.nanolett.3c00045 Read Online

ACCESS | Metrics & More | Article Recommendations | Supporting Information

ABSTRACT: In this Letter, we provide experimental evidence of the time-reversal symmetric Hall effect in a mesoscopic system, namely, high-mobility graphene−WSe_2 heterostructures. This linear, dissipative Hall effect, whose sign depends on the sign of the charge carriers, persists up to room temperature. The magnitude and the sign of the Hall signal can be tuned using an external perpendicular electric field. Our joint experimental and theoretical study establishes that the strain induced by lattice mismatch, or alignment angle inhomogeneity, produces anisotropic bands in graphene while simultaneously breaking the inversion symmetry. The band anisotropy and reduced spatial symmetry lead to the appearance of a time-reversal symmetric Hall effect. Our study establishes graphene−transition metal dichalcogenide-based heterostructures as an excellent platform for studying the effects of broken symmetry on the physical properties of band-engineered two-dimensional systems.

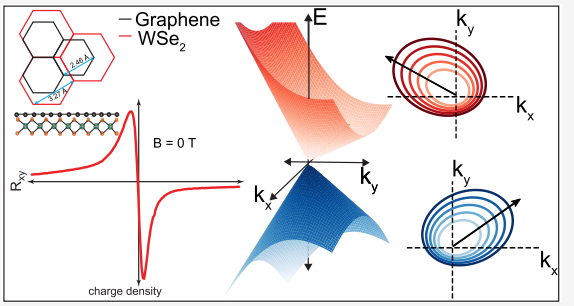

KEYWORDS: *graphene, WSe_2, symmetric Hall effect, time-reversal symmetry, strain, band anisotropy*

Topological and band geometric effects in two-dimensional systems have attracted significant attention due to their fascinating physics and potential applications in spintronics and novel electronic devices.[1−5] Graphene-based heterostructures offer one such exciting platform for studying band geometric effects. The coupling to the charge, spin, and valley degrees of freedom in graphene leads to, among other things, a multitude of unconventional Hall effects; some prominent examples include the spin Hall,[6−9] the valley Hall,[10−15] the nonlinear anomalous Hall,[16−22] and the layer contrasted Hall effect.[3,23] All of these phases require a finite Berry curvature and opposite anomalous velocity in the two valleys of graphene to exist.[16−18] They fall under the category of dissipationless antisymmetric Hall effect, in which the current always flows perpendicular to the electric field, and the polarity of voltage changes if one interchanges the source and drain contacts. What is underappreciated is that a time-reversal symmetric system with anisotropic band velocity can also host nontrivial and symmetric Hall effects irrespective of the presence or absence of a finite Berry curvature. The focus of this Letter is the observation of a finite "symmetric Hall response".[24−26] The symmetric Hall effect can appear without time-reversal symmetry breaking, and it is unrelated to the so-called quantum geometry of the wave function.

In this Letter, we report the observation of a large time-reversal symmetric, linear Hall response $R_{xy}(B = 0)$ originating from asymmetric momentum space band dispersion of the heterostructure. We find that the sign of $R_{xy}(B = 0)$ flips as the Fermi level moves from the valence to the conduction band (mimicking the finite B field classical Hall signal in graphene) and is observed up to room temperature. We explain our observations using a realistic two-band model for an anisotropic band dispersion with an orthogonal anisotropy orientation in the two bands.

Single-layer WSe_2 used as a substrate influences the graphene bands in two significant ways. The first of these has been well studied. Graphene on WSe_2 possesses spin-split bands owing to the Ising-like SOC, which gives rise to the spin Hall effect.[27−29] The second effect, equally vital for our purposes but little explored to date, is the appearance of a substantial lateral strain in the graphene layer. We show that the effect of this proximity-induced SOC, lattice mismatch, and small angle rotation can induce gap and asymmetric dispersion in graphene, leading to the appearance of a symmetric Hall signal near the Dirac point. We verify that the symmetric, charge-carrier sign-dependent Hall response is absent in graphene devices without the WSe_2 layer. Note that previous studies of the SLG−WSe_2 heterostructure (or graphene on transition metal dichalcogenides in general) focused primarily

Received: January 4, 2023
Revised: July 17, 2023

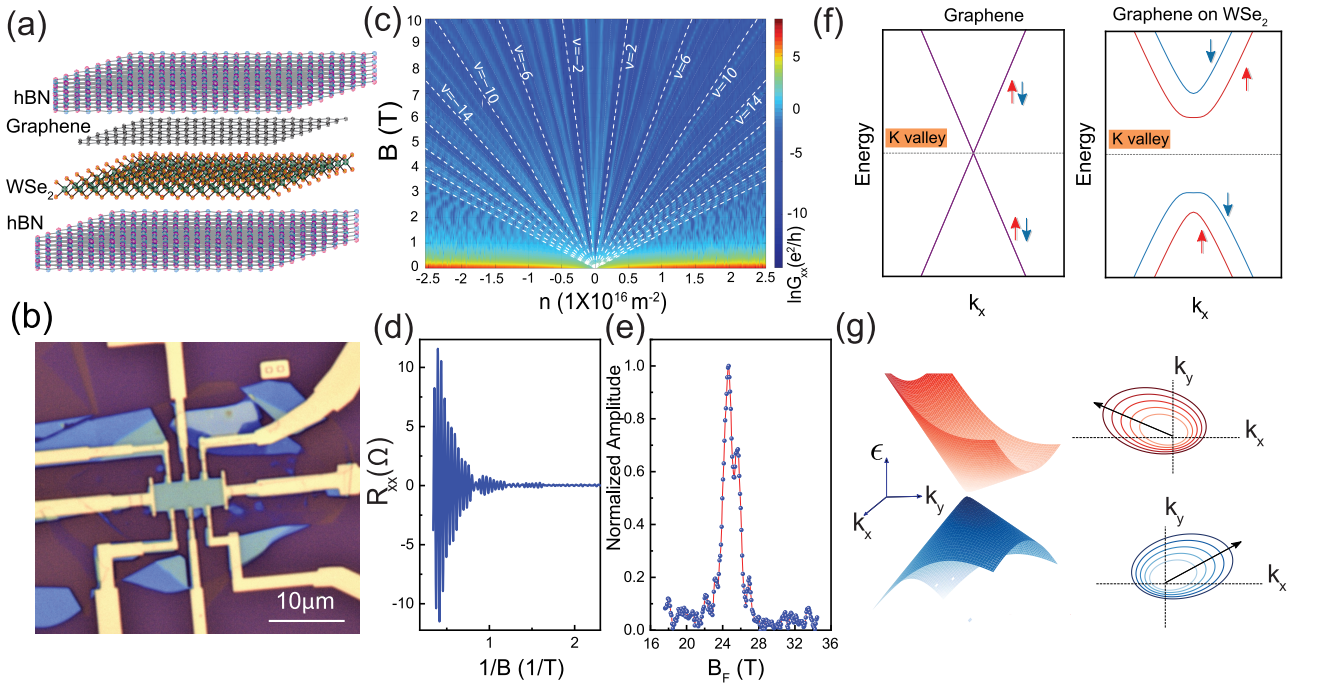

Figure 1. Device characteristics and band dispersion. (a) Schematic of the graphene−WSe_2 layers encapsulated in hBN illustrating the sequence of crystal stacking. (b) Optical image of the device. (c) Map of the longitudinal conductance $[G_{xx}(B)]$ with varying carrier density n and perpendicular magnetic field B at ∼20 mK. The thicker dashed lines correspond to the signature plateaus of single-layer graphene. Thinner lines mark the broken-symmetry phases indicating complete lifting of the spin and valley degeneracies at low B values. (d) SdH oscillations vs $1/B$ at a V_{bg} of −40 V. (e) Fourier spectrum of the SdH oscillations. Two peaks are distinctly visible, establishing the presence of two Fermi surfaces. (f) Schematic of the band dispersion of the K valley of monolayer graphene (left) and graphene on the WSe_2 heterostructure (right). The WSe_2 layer essentially lifts the spin degeneracy of the low-lying energy bands and opens a gap at the Fermi energy. (g) Schematic of the band structure of strained graphene on WSe_2 with the orientation of band anisotropy being orthogonal in the conduction and valence bands. This is highlighted by the arrows in the contour plots.

on the spin aspects of the transport,[27,28,30−32] where a nonlocal signal is measured as a signature of the spin Hall effect and weak (anti) localization measurements were used to quantify the spin−orbit coupling strength.[29,33−39] Interestingly, these studies did not probe the finite Hall effect without a magnetic field. This makes our observation of the time-reversal symmetric nontrivial Hall effect in this system unique.

Heterostructures of single-layer graphene (SLG) and single-layer WSe_2, encapsulated by crystalline hexagonal boron nitrate (hBN), were fabricated using a dry transfer technique.[40,41] One-dimensional electrical contacts were formed by electron beam lithography, followed by etching (using a mixture of CHF_3 and O_2) and deposition of 5 nm/60 nm Cr/Au contacts. A separate deposition was done for the top-gate electrode (see the Supporting Information for details). A schematic of the device structure is shown in Figure 1a, and an optical image of the device is shown in Figure 1b. The dual-gated architecture of the devices allows independent control of charge-carrier density n and vertical displacement field D/ε_0; $n = (C_{tg}V_{tg} + C_{bg}V_{bg})/e - n_0$ and $D = (C_{tg}V_{tg} - C_{bg}V_{bg})/2 - D_0$. Here C_{bg} (C_{tg}) is the capacitance per unit area of the back gate (top gate), and V_{bg} (V_{tg}) is the back-gate (top-gate) bias. n_0 and D_0 are the residual charge-carrier density and residual vertical displacement field induced by impurities in the device channel, respectively.

Electrical transport measurements were performed at a source-drain current of 10 nA using low-frequency lock-in detection techniques. All data were obtained at 20 mK unless specified otherwise. The measurements were performed on multiple devices; the results were similar. In the text, we present the data from a single device, SW1, unless specified. The data from other devices (SW2, SG3, SG4, and SW3) are shown in Figures S5−S9.

A map of the measured longitudinal conductance G_{xx} as a function of charge-carrier density n and perpendicular magnetic field B is shown in Figure 1c. The appearance of broken symmetry quantum Hall states at low B fields implies complete lifting of the spin and valley degeneracies in SLG bands. The splitting of the spin-degenerate bands in SLG (shown schematically in Figure 1f) is also evident from the beating pattern seen in the Shubnikov de Haas oscillations (Figure 1d) and the double periodicity in the corresponding Fourier spectrum (Figure 1e). This beating pattern is absent in SLG devices without WSe_2 (see section S10).

Figure 1g is a schematic representation of the band structure of strained graphene on WSe_2 with the orientation of the band anisotropy in the valence and conduction band being orthogonal (see section S1 for details). The lifting of spin and valley degeneracies in the band dispersion (along with the high field effect mobility $\mu \sim 140\,000$ cm^2 V^{-1} s^{-1} of the device) shows that the graphene−WSe_2 interface is atomically clean with significant interfacial coupling and minimal random potential fluctuations.

In Figure 2a, we present the data for longitudinal resistance R_{xx} (left axis, red line) and transverse resistance R_{xy} (right axis, blue line), measured at 0 T. We observe a finite Hall signal in a narrow range of charge-carrier densities $\Delta n = \pm 10^{15}$ m^{-2} centered about the charge neutrality point. $R_{xy}(B = 0)$ values measured for other contact configurations give quantitatively similar results (see Figure S5). Strikingly, $R_{xy}(B = 0)$ features a

https://doi.org/10.1021/acs.nanolett.3c00045
Nano Lett. XXXX, XXX, XXX−XXX

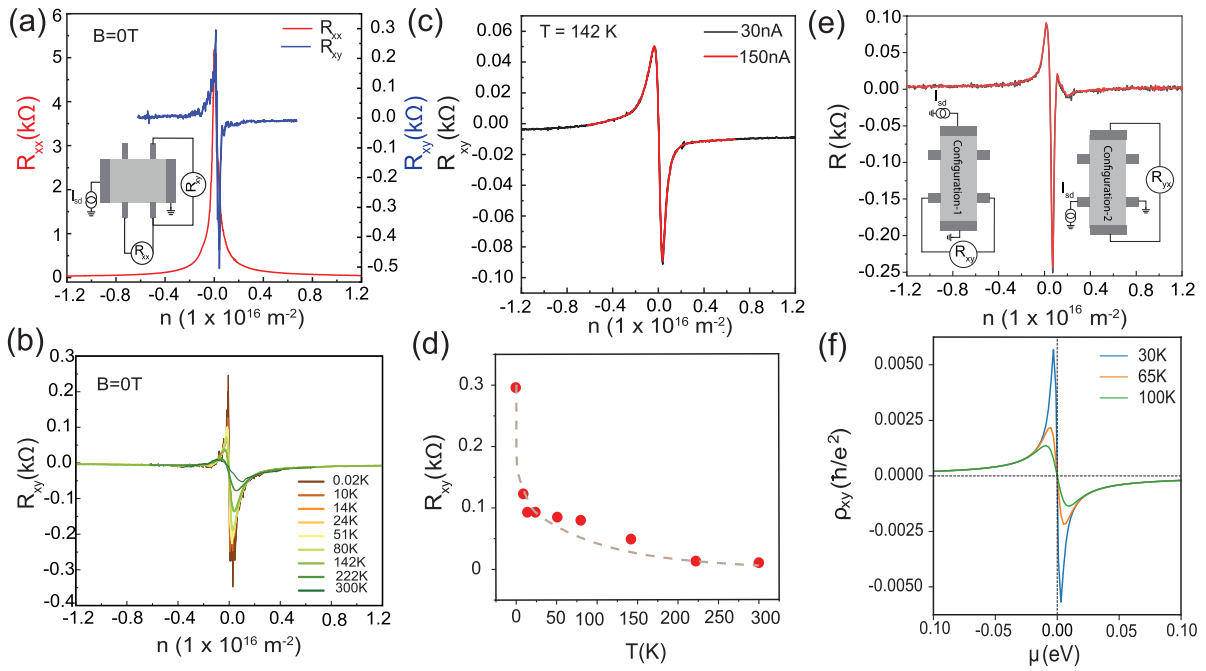

Figure 2. Sign-reversal symmetric Hall effect. (a) Plots of zero-magnetic field longitudinal resistance $R_{xx}(B = 0)$ (left axis, red line) and zero-magnetic field transverse resistance $R_{xy}(B = 0)$ (right axis, blue line) vs n. The data were measured at 20 mK. (b) $R_{xy}(B = 0)$ response as a function of n at a few representative temperatures. The measured $R_{xy}(B = 0)$ persists up to 300 K. (c) Plot of $R_{xy}(B = 0)$ as a function of n for two different values of electrical current. The data were taken at 142 K. (d) Plot of the peak value of $R_{xy}(B = 0)$ vs T. The dotted line is a guide to the eye. (e) Plot of the transverse resistance vs number density in two different configurations for device SW2. Configuration 1 measures $R_{xy}(B = 0)$, and configuration 2 measures $R_{yx}(B = 0)$. One can see that $R_{xy}(B = 0) = R_{yx}(B = 0)$; the measured Hall effect is symmetric upon interchanging the voltage and current leads. (f) Theoretically calculated symmetric Hall resistivity (ρ_{xy}) for three different temperatures.

change in the sign about the charge neutrality point; it is positive when $n < 0$ (hole band) and negative when $n > 0$ (electron band). The current independence of $R_{xy}(B = 0)$ establishes it to be a linear Hall effect (Figure 2c). The finite Hall response persists up to room temperature with a diminished amplitude, as shown in panels b and d of Figure 2. Importantly, the transverse signal is symmetric upon exchange of the voltage and current leads; $R_{xy}(B = 0) = R_{yx}(B = 0)$ (see Figure 2e). This observation in hBN−graphene−WSe_2−hBN heterostructures of a room-temperature, $B = 0$ symmetric Hall effect that changes sign across the charge neutrality point is unique and is our central result.

A finite zero-magnetic field Hall response is often seen in graphene devices near the charge neutrality point (see Figure S7). This can originate from trivial effects that mix the longitudinal and transverse signals (e.g., misaligned probes or misalignment of the measurement axis with the crystal axis); thus, the sign of this signal is independent of the type of charge carrier. We emphasize that our observation is distinct from this trivial case in one very important aspect. In graphene−WSe_2 heterostructures, the sign of the Hall response flips as the carrier type changes from electrons to holes (see section S8 for a comparison of the data in graphene and graphene−WSe_2 devices). The data for $R_{xy}(B = 0)$ were also reproduced in cryostats without a superconducting magnet, ruling out the remnant field of a magnet as the origin of the observed Hall response. Measurement of $R_{xy}(B = 0)$ in a device with contacts in the "sunflower" geometry shows that the symmetric Hall effect is anisotropic with a strong angle dependence (see section S9).

Having ruled out experimental artifacts as the origin of our unusual observation, we develop below a detailed model that explains our essential observations. A symmetric Hall response can arise from the Drude mechanism in materials with an anisotropic band dispersion. The symmetric Hall conductivity is specified as[24,42] $\sigma_{xy} = e^2\tau\int_k v_x v_y(-f')$, where $v_i = \partial_{k_i}\varepsilon$ is the band velocity, f' is the energy derivative of the Fermi distribution function, and τ is the scattering time. However, such a symmetric Hall response usually does not change its sign when going from the valence to the conduction band, contrary to our experimental observations (see Figure S6). We argue below that such sign reversal can arise in particle−hole symmetry broken systems with different anisotropy orientations in the electronic dispersion of the conduction and valence band.

To gain a complete understanding of the unusual Hall effect observed in the SLG−WSe_2 structure, we start by noting that the band structure of this system is anisotropic. This is schematically highlighted in Figure 1g. The anisotropy axis in the conduction and valence bands is close to orthogonal (see Figure S1 for realistic calculations for the graphene−WSe_2 heterostructure). This band structure is reminiscent of that seen in periodically strained bilayer graphene that hosts a time-reversal symmetric linear pseudoplanar Hall effect.[24] Such an anisotropic band dispersion preserves time-reversal symmetry but breaks particle−hole symmetry (see the Supporting Information for details). Let us consider a symmetric system to which we add a small anisotropy. The anisotropy modifies the band structure to induce a change in the band velocity, $v_{x/y} \rightarrow v_{x/y}^{\mathrm{symm}} + \delta v_{x/y}$. In a simplistic scenario in which $\delta v_{x/y}$ are independent of the Bloch momentum, we have $\sigma_{xy} \propto \delta v_x \delta v_y |\mu|$. One can show that if the tilt directions of the conduction and valence bands are orthogonal to each other, as they are for the SLG−WSe_2 structure (see Figure 1e), the product $\delta v_x \delta v_y$ and

https://doi.org/10.1021/acs.nanolett.3c00045
Nano Lett. XXXX, XXX, XXX−XXX

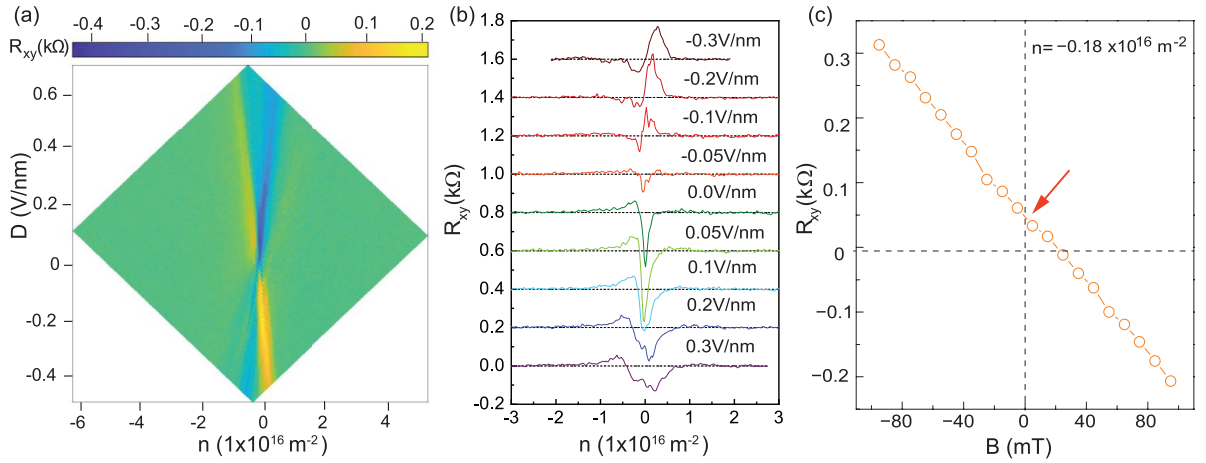

Figure 3. Dependence of transverse resistance R_{xy} on D and B. (a) Two-dimensional contour map of $R_{xy}(B = 0)$ plotted in the $n-D$ plane. (b) Plots of $R_{xy}(B = 0)$ vs n for different values of D. The data have been vertically shifted by 200 Ω for the sake of clarity. The dashed horizontal line for each plot marks the zero point of $R_{xy}(B = 0)$. (c) Representative plot of R_{xy} vs B measured at $n = -0.18 \times 10^{16}$ m^{-2}. An arrow marks the value of the anomalous Hall resistance.

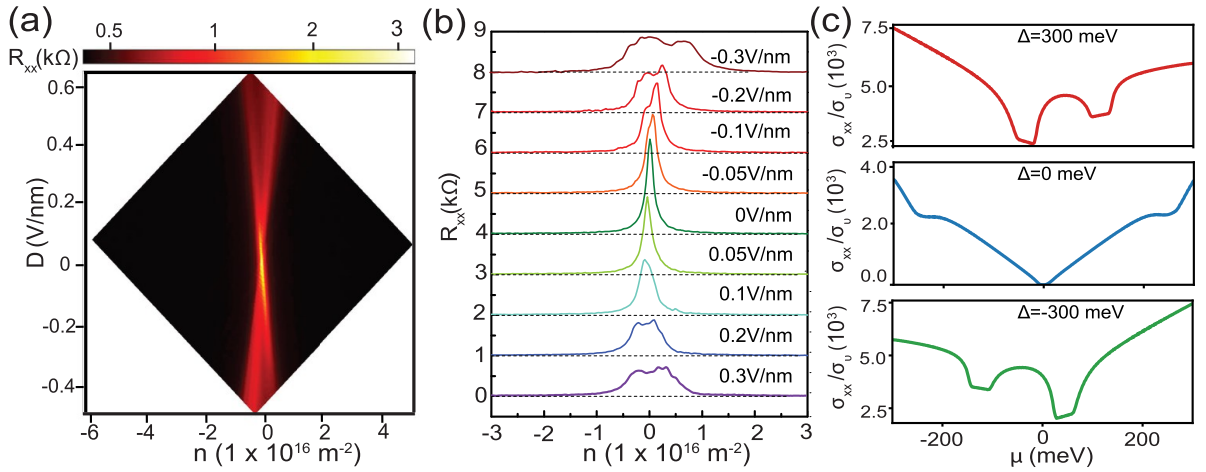

Figure 4. Dependence of $R_{xx}(B = 0)$ on D. (a) Two-dimensional contour map of $R_{xx}(B = 0)$ plotted in the $n-D$ plane. (b) Plots of $R_{xx}(B = 0)$ vs n for different values of D. The data have been vertically shifted by 1 kΩ for the sake of clarity. The dashed horizontal line for each plot is the zero point of the y-axis. (c) Variation of the calculated Drude conductivity σ_{xx} with energy (μ) for three different values of the interlayer potential induced by an applied electric field: Δ = 300 meV (red line), Δ = 0 meV (blue line), and Δ = −300 meV (green line). The values of σ_{xx} have been scaled by σ_v, where $\sigma_v = e^2\tau/4\pi^2\hbar^2$.

consequently the symmetric Hall response reverse their signs as we go from the conduction to valence band.

This orthogonal orientation of the band anisotropy in the conduction and valence bands is the origin of the sign-reversal symmetric Hall effect (see the Supporting Information for the generic model of the sign-reversal symmetric Hall effect and detailed calculations for the graphene−WSe_2 heterostructure). Figure 2f presents the calculated symmetric Hall conductivity for an effective two-band model, which qualitatively captures the experimentally observed sign-reversal symmetric Hall effect (also see Figure S2).

We do not find evidence of a sign-reversal symmetric Hall effect in hBN−SLG−hBN devices without the intervening WSe_2 layer (Figure S7). Thus, the orthogonal asymmetry in the conduction and valence bands induced by the WSe_2−graphene combination is essential for this effect.

The band anisotropy in SLG on WSe_2 can be traced back to the lattice mismatch-induced strain. The lattice constant of graphene is ∼2.46 Å, while that of WSe_2 is ∼3.27 Å. This large lattice mismatch generates a significant strain across the graphene flake as the heterostructure relaxes to the stable ground state. From Raman spectroscopy, we estimate the magnitude of the strain on the SLG layer in our hBN−SLG−WSe_2−hBN heterostructure to be ≈0.15−0.20% (see section S5). We find that the strain magnitude decreases with temperature (see section S5 for details). Our observed symmetric Hall effect survives the combined action of (i) decreases in strain and band anisotropy with an increase in temperature and (ii) the thermal broadening of the Fermi function to be finite at room temperature.

Having demonstrated the symmetric Hall effect, we now focus on the dependence of the symmetric Hall response on perpendicular displacement field D (Figure 3). It is illuminating to map transverse zero-B field conductivity $R_{xy}(B = 0)$ data in the $n-D$ plane (Figure 3a). The plot shows that $R_{xy}(B = 0)$ is finite only at the band edges. This can be seen clearly in the line plots of $R_{xy}(B = 0)$ for different values of D shown in Figure 3b. Note that the plots are vertically offset by 200 Ω for the sake of clarity. The measured

https://doi.org/10.1021/acs.nanolett.3c00045
Nano Lett. XXXX, XXX, XXX−XXX

$R_{xy}(B = 0)$ has an intriguing D dependence; it changes its sign as the direction of D flips (Figure 3a,b).

Measurements in a finite magnetic field B applied perpendicular to the device interface (see the Supporting Information) reveal the interplay between the classical Hall effect and the $B = 0$ symmetric Hall effect. The data smoothly cross over from the symmetric Hall phase at $B = 0$ to the conventional Hall phase at a finite B field with an anti-crossing feature. This feature resembles the planar Hall effect in corrugated bilayer graphene.[24] A non-zero intercept of the plot of R_{xy} versus B (shown for a fixed n in Figure 3c) on the B axis captures the symmetric Hall effect. We note that R_{xy} is nonhysteretic in the presence of a small nonquantizing magnetic field (see Figure S6d), ruling out emergent ferromagnetism in the system.

In Figure 4a, we present a plot of R_{xx} in the $n-D$ plane measured at $B = 0$. We observe that with an increase in D, the resistance peak at the charge neutrality point splits into two maxima. This feature can be better appreciated in Figure 4b, where we show individual plots of $R_{xx}(B = 0)$ versus n at several representative values of D. At higher values of $|D|$, we find two distinct peaks in R_{xx} separated by a shallow valley. Such a displacement field-dependent dispersion of the bands near the Dirac point is not captured by the existing models for graphene–WSe_2 heterostructures.[33,43−49] To remedy this, we construct a new model Hamiltonian for the graphene–WSe_2 system, retaining both the WSe_2 and the graphene Hamiltonian blocks, which allows us to include the impact of a vertical displacement field systematically (see the Supporting Information for details). Figure 4c is a plot of the theoretically calculated σ_{xx} as a function of the chemical potential; the panels show the splitting of the conductivity minima into two asymmetric conductivity minima at a finite D value. Our model thus reproduces the prominent features of σ_{xx} both at a zero displacement field[43,45] and at a finite D, along with the observed symmetric Hall effect.

To summarize, we report the first observation of a room-temperature time-reversal symmetric Hall effect in high-mobility graphene–WSe_2 heterostructures. Primarily known for their promising spintronic aspects, the charge Hall response of such a heterostructure was expected to be relatively mundane. On the contrary, we measure a time-reversal symmetric Hall effect at zero magnetic field. More interestingly, the observed symmetric Hall effect changes sign across the charge neutrality point and persists until room temperature. We show that the symmetric Hall effect arises from the anisotropy of the electronic band structure. The sign reversal of the observed Hall effect arises from the different orientation of the anisotropy direction in the conduction and valence bands. The symmetric Hall response features a unique perpendicular electric field tunability. Our work establishes the graphene–WSe_2 heterostructure as an excellent platform for further exploration of the interplay of charge, spin, and valley responses in band-engineered two-dimensional systems.

■ ASSOCIATED CONTENT

Supporting Information

The Supporting Information is available free of charge at https://pubs.acs.org/doi/10.1021/acs.nanolett.3c00045.

Detailed discussions of the (a) model Hamiltonian of the graphene–WSe_2 heterostructure, (b) generic low-energy model for the sign-reversal symmetric Hall effect, (c) Drude longitudinal conductivity, (d) device fabrication, (e) Raman shift and strain, (e) additional data for the symmetric Hall effect on device SW1, (f) additional data for the symmetric Hall effect on device SW2, (g) transverse resistance data of the hBN–graphene–hBN device at $B = 0$, (h) comparison of SdH oscillations in bare graphene and SLG–WSe_2 devices, and (i) angle dependence of the measured symmetric Hall effect (PDF)

■ AUTHOR INFORMATION

Corresponding Authors

Amit Agarwal − *Department of Physics, Indian Institute of Technology Kanpur, Kanpur 208016, India*; Email: amitag@iitk.ac.in

Aveek Bid − *Department of Physics, Indian Institute of Science, Bangalore 560012, India*; orcid.org/0000-0002-2378-7980; Email: aveek@iisc.ac.in

Authors

Priya Tiwari − *Department of Physics, Indian Institute of Science, Bangalore 560012, India; Braun Center for Submicron Research, Department of Condensed Matter Physics, Weizmann Institute of Science, Rehovot 7610001, Israel*

Divya Sahani − *Department of Physics, Indian Institute of Science, Bangalore 560012, India*

Atasi Chakraborty − *Department of Physics, Indian Institute of Technology Kanpur, Kanpur 208016, India; Institute of Physics, Johannes Gutenberg Universität, 55128 Mainz, Germany*

Kamal Das − *Department of Physics, Indian Institute of Technology Kanpur, Kanpur 208016, India; Department of Condensed Matter Physics, Weizmann Institute of Science, Rehovot 7610001, Israel*

Kenji Watanabe − *Research Center for Functional Materials, National Institute for Materials Science, Tsukuba 305-0044, Japan*; orcid.org/0000-0003-3701-8119

Takashi Taniguchi − *International Center for Materials Nanoarchitectonics, National Institute for Materials Science, Tsukuba 305-0044, Japan*; orcid.org/0000-0002-1467-3105

Complete contact information is available at: https://pubs.acs.org/10.1021/acs.nanolett.3c00045

Author Contributions

P.T. and D.S. contributed equally to this work. A.B., P.T., and D.S. conceptualized the study, performed the measurements, and analyzed the data. A.A., A.C., and K.D. performed the theoretical analysis. K.W. and T.T. grew the hBN single crystals. All of the authors contributed to the preparation of the manuscript.

Notes

The authors declare no competing financial interest.

■ ACKNOWLEDGMENTS

A.B. acknowledges funding from the Department of Science & Technology FIST program, DST fellowship (DST/SJF/PSA01/2016-17), and the U.S. Army DEVCOM Indo-Pacific (Project FA5209 22P0166). A.C. acknowledges the Indian Institute of Technology Kanpur and the Science and Engineering Research Board (SERB) National Postdoctoral

Fellowship (PDF/2021/000346), India, for partial financial support. A.C. acknowledges an Alexander Von Humboldt Postdoctoral fellowship, Germany, for funding. A.A. acknowledges the Science and Engineering Research Board for Project MTR/2019/001520 and the Department of Science and Technology for Project DST/NM/TUE/QM-6/2019(G)-IIT Kanpur of the Government of India for funding. K.W. and T.T. acknowledge support from JSPS KAKENHI (Grants 19H05790, 20H00354, and 21H05233). The authors acknowledge stimulating discussions with Sumanta Tewari and Jay Deep Sau.

REFERENCES

(1) Xiao, D.; Chang, M.-C.; Niu, Q. Berry phase effects on electronic properties. *Rev. Mod. Phys.* **2010**, *82*, 1959−2007.
(2) Ahn, J.; Guo, G.-Y.; Nagaosa, N.; Vishwanath, A. Riemannian geometry of resonant optical responses. *Nat. Phys.* **2022**, *18*, 290−295.
(3) Gao, A.; et al. Layer Hall effect in a 2D topological axion antiferromagnet. *Nature* **2021**, *595*, 521−525.
(4) Bhalla, P.; Das, K.; Culcer, D.; Agarwal, A. Resonant Second-Harmonic Generation as a Probe of Quantum Geometry. *Phys. Rev. Lett.* **2022**, *129*, 227401.
(5) Han, W.; Kawakami, R. K.; Gmitra, M.; Fabian, J. Graphene spintronics. *Nat. Nanotechnol.* **2014**, *9*, 794−807.
(6) Sinova, J.; Valenzuela, S. O.; Wunderlich, J.; Back, C.; Jungwirth, T. Spin hall effects. *Reviews of modern physics* **2015**, *87*, 1213.
(7) Hirsch, J. Spin hall effect. *Physical review letters* **1999**, *83*, 1834.
(8) Bernevig, B. A.; Zhang, S.-C. Quantum spin Hall effect. *Physical review letters* **2006**, *96*, 106802.
(9) Tiwari, P.; Jat, M. K.; Udupa, A.; Narang, D. S.; Watanabe, K.; Taniguchi, T.; Sen, D.; Bid, A. Experimental observation of spin-split energy dispersion in high-mobility single-layer graphene/WSe2 heterostructures. *npj 2D Mater. Appl.* **2022**, *6*, 68.
(10) Xiao, D.; Liu, G.-B.; Feng, W.; Xu, X.; Yao, W. Coupled Spin and Valley Physics in Monolayers of MoS_2 and Other Group-VI Dichalcogenides. *Phys. Rev. Lett.* **2012**, *108*, 196802.
(11) Cresti, A.; Nikolić, B. K.; García, J. H.; Roche, S. Charge, spin and valley Hall effects in disordered graphene. *Riv. Nuovo Cimento* **2016**, *39*, 587−667.
(12) Mak, K. F.; McGill, K. L.; Park, J.; McEuen, P. L. The valley Hall effect in MoS2 transistors. *Science* **2014**, *344*, 1489−1492.
(13) Lee, J.; Mak, K. F.; Shan, J. Electrical control of the valley Hall effect in bilayer MoS2 transistors. *Nature Nanotechnol.* **2016**, *11*, 421−425.
(14) Liu, J.; Ma, Z.; Gao, J.; Dai, X. Quantum valley Hall effect, orbital magnetism, and anomalous Hall effect in twisted multilayer graphene systems. *Physical Review X* **2019**, *9*, 031021.
(15) Qiao, Z.; Yang, S. A.; Feng, W.; Tse, W.-K.; Ding, J.; Yao, Y.; Wang, J.; Niu, Q. Quantum anomalous Hall effect in graphene from Rashba and exchange effects. *Phys. Rev. B* **2010**, *82*, 161414.
(16) Shimazaki, Y.; Yamamoto, M.; Borzenets, I. V.; Watanabe, K.; Taniguchi, T.; Tarucha, S. Generation and detection of pure valley current by electrically induced Berry curvature in bilayer graphene. *Nat. Phys.* **2015**, *11*, 1032−1036.
(17) Sui, M.; Chen, G.; Ma, L.; Shan, W.-Y.; Tian, D.; Watanabe, K.; Taniguchi, T.; Jin, X.; Yao, W.; Xiao, D.; Zhang, Y. Gate-tunable topological valley transport in bilayer graphene. *Nat. Phys.* **2015**, *11*, 1027−1031.
(18) Wallbank, J. R.; et al. Tuning the valley and chiral quantum state of Dirac electrons in van der Waals heterostructures. *Science* **2016**, *353*, 575−579.
(19) Sodemann, I.; Fu, L. Quantum Nonlinear Hall Effect Induced by Berry Curvature Dipole in Time-Reversal Invariant Materials. *Phys. Rev. Lett.* **2015**, *115*, 216806.
(20) Du, Z. Z.; Wang, C. M.; Li, S.; Lu, H.-Z.; Xie, X. C. Disorder-induced nonlinear Hall effect with time-reversal symmetry. *Nat. Commun.* **2019**, *10*, 3047.
(21) Sinha, S.; Adak, P. C.; Chakraborty, A.; Das, K.; Debnath, K.; Sangani, L. D. V.; Watanabe, K.; Taniguchi, T.; Waghmare, U. V.; Agarwal, A.; Deshmukh, M. M. Berry curvature dipole senses topological transition in a moiré superlattice. *Nat. Phys.* **2022**, *18*, 765−770.
(22) Chakraborty, A.; Das, K.; Sinha, S.; Adak, P. C.; Deshmukh, M. M.; Agarwal, A. Nonlinear anomalous Hall effects probe topological phase-transitions in twisted double bilayer graphene. *2D Materials* **2022**, *9*, 045020.
(23) Zhai, D.; Chen, C.; Xiao, C.; Yao, W. Time-reversal even charge hall effect from twisted interface coupling. *Nat. Commun.* **2023**, *14*, 1961.
(24) Ho, S.-C.; Chang, C.-H.; Hsieh, Y.-C.; Lo, S.-T.; Huang, B.; Vu, T.-H.-Y.; Ortix, C.; Chen, T.-M. Hall effects in artificially corrugated bilayer graphene without breaking time-reversal symmetry. *Nature Electronics* **2021**, *4*, 116−125.
(25) Nandy, S.; Sharma, G.; Taraphder, A.; Tewari, S. Chiral anomaly as the origin of the planar Hall effect in Weyl semimetals. *Physical review letters* **2017**, *119*, 176804.
(26) Kumar, N.; Guin, S. N.; Felser, C.; Shekhar, C. Planar Hall effect in the Weyl semimetal GdPtBi. *Phys. Rev. B* **2018**, *98*, 041103.
(27) Avsar, A.; Tan, J. Y.; Taychatanapat, T.; Balakrishnan, J.; Koon, G.; Yeo, Y.; Lahiri, J.; Carvalho, A.; Rodin, A.; O'Farrell, E.; et al. Spin-orbit proximity effect in graphene. *Nat. Commun.* **2014**, *5*, 4875.
(28) Ghiasi, T. S.; Kaverzin, A. A.; Blah, P. J.; van Wees, B. J. Charge-to-spin conversion by the Rashba-Edelstein effect in two-dimensional van der Waals heterostructures up to room temperature. *Nano Lett.* **2019**, *19*, 5959−5966.
(29) Tiwari, P.; Srivastav, S. K.; Ray, S.; Das, T.; Bid, A. Observation of Time-Reversal Invariant Helical Edge-Modes in Bilayer Graphene/WSe2 Heterostructure. *ACS Nano* **2021**, *15*, 916−922.
(30) Herling, F.; Safeer, C. K.; Ingla-Aynés, J.; Ontoso, N.; Hueso, L. E.; Casanova, F. Gate tunability of highly efficient spin-to-charge conversion by spin Hall effect in graphene proximitized with WSe2. *APL Mater.* **2020**, *8*, 071103.
(31) Dastgeer, G.; Afzal, A. M.; Jaffery, S. H. A.; Imran, M.; Assiri, M. A.; Nisar, S. Gate modulation of the spin current in graphene/WSe2 van der Waals heterostructure at room temperature. *J. Alloys Compd.* **2022**, *919*, 165815.
(32) Lee, S.; de Sousa, D. J. P.; Kwon, Y.-K.; de Juan, F.; Chi, Z.; Casanova, F.; Low, T. Charge-to-spin conversion in twisted graphene/WSe_2 heterostructures. *Phys. Rev. B* **2022**, *106*, 165420.
(33) Wang, Z.; Ki, D.-K.; Chen, H.; Berger, H.; MacDonald, A. H.; Morpurgo, A. F. Strong interface-induced spin−orbit interaction in graphene on WS2. *Nat. Commun.* **2015**, *6*, 8339.
(34) Wang, Z.; Ki, D.-K.; Khoo, J. Y.; Mauro, D.; Berger, H.; Levitov, L. S.; Morpurgo, A. F. Origin and Magnitude of 'Designer' Spin-Orbit Interaction in Graphene on Semiconducting Transition Metal Dichalcogenides. *Phys. Rev. X* **2016**, *6*, 041020.
(35) Völkl, T.; Rockinger, T.; Drienovsky, M.; Watanabe, K.; Taniguchi, T.; Weiss, D.; Eroms, J. Magnetotransport in heterostructures of transition metal dichalcogenides and graphene. *Phys. Rev. B* **2017**, *96*, 125405.
(36) Wakamura, T.; Reale, F.; Palczynski, P.; Zhao, M. Q.; Johnson, A. T. C.; Guéron, S.; Mattevi, C.; Ouerghi, A.; Bouchiat, H. Spin-orbit interaction induced in graphene by transition metal dichalcogenides. *Phys. Rev. B* **2019**, *99*, 245402.
(37) Fülöp, B.; Márffy, A.; Zihlmann, S.; Gmitra, M.; Tóvári, E.; Szentpéteri, B.; Kedves, M.; Watanabe, K.; Taniguchi, T.; Fabian, J.; Schönenberger, C.; Makk, P.; Csonka, S. Boosting proximity spin−orbit coupling in graphene/WSe2 heterostructures via hydrostatic pressure. *npj 2D Mater. Appl.* **2021**, *5*, 82.
(38) Tiwari, P.; Srivastav, S. K.; Bid, A. Electric-Field-Tunable Valley Zeeman Effect in Bilayer Graphene Heterostructures: Realization of the Spin-Orbit Valve Effect. *Phys. Rev. Lett.* **2021**, *126*, 096801.
(39) Tiwari, P.; Srivastav, S. K.; Bid, A. Electric-Field-Tunable Valley Zeeman Effect in Bilayer Graphene Heterostructures: Realization of the Spin-Orbit Valve Effect. *Phys. Rev. Lett.* **2021**, *126*, 096801.

https://doi.org/10.1021/acs.nanolett.3c00045
Nano Lett. XXXX, XXX, XXX−XXX

(40) Pizzocchero, F.; Gammelgaard, L.; Jessen, B. S.; Caridad, J. M.; Wang, L.; Hone, J.; Bøggild, P.; Booth, T. J. The hot pick-up technique for batch assembly of van der Waals heterostructures. *Nat. Commun.* **2016**, *7*, 11894.
(41) Wang, L.; Meric, I.; Huang, P.; Gao, Q.; Gao, Y.; Tran, H.; Taniguchi, T.; Watanabe, K.; Campos, L.; Muller, D.; et al. One-dimensional electrical contact to a two-dimensional material. *Science* **2013**, *342*, 614−617.
(42) Ashcroft, N. W.; Mermin, N. D. *Solid State Physics*; Holt-Saunders, 1976.
(43) Gmitra, M.; Kochan, D.; Högl, P.; Fabian, J. Trivial and inverted Dirac bands and the emergence of quantum spin Hall states in graphene on transition-metal dichalcogenides. *Phys. Rev. B* **2016**, *93*, 155104.
(44) Offidani, M.; Milletarì, M.; Raimondi, R.; Ferreira, A. Optimal Charge-to-Spin Conversion in Graphene on Transition-Metal Dichalcogenides. *Phys. Rev. Lett.* **2017**, *119*, 196801.
(45) Cummings, A. W.; Garcia, J. H.; Fabian, J.; Roche, S. Giant Spin Lifetime Anisotropy in Graphene Induced by Proximity Effects. *Phys. Rev. Lett.* **2017**, *119*, 206601.
(46) Garcia, J. H.; Vila, M.; Cummings, A. W.; Roche, S. Spin transport in graphene/transition metal dichalcogenide heterostructures. *Chem. Soc. Rev.* **2018**, *47*, 3359−3379.
(47) Li, Y.; Koshino, M. Twist-angle dependence of the proximity spin-orbit coupling in graphene on transition-metal dichalcogenides. *Phys. Rev. B* **2019**, *99*, 075438.
(48) Zubair, M.; Vasilopoulos, P.; Tahir, M. Influence of interface induced valley-Zeeman and spin-orbit couplings on transport in heterostructures of graphene on WSe_2. *Phys. Rev. B* **2020**, *101*, 165436.
(49) Kumar, A.; Maiti, S.; Maslov, D. L. Zero-field spin resonance in graphene with proximity-induced spin-orbit coupling. *Phys. Rev. B* **2021**, *104*, 155138.

https://doi.org/10.1021/acs.nanolett.3c00045
Nano Lett. XXXX, XXX, XXX−XXX